

Parametric Design of Parabolic Reflector Antenna with Switchable Cosecant-Squared Pattern

Ahmet S. Turk¹ and Okan Yurduseven^{1,2}

¹Department of Electronics and Communication Engineering
Yıldız Technical University, Besiktas, Istanbul, 34349, Turkey
asturk@yildiz.edu.tr

²Department of Electrical and Electronics Engineering
Marmara University, Goztepe, Istanbul, 34722, Turkey
oyurduseven@marmara.edu.tr

Abstract - This paper deals with the parametric analysis of multi-beam parabolic reflector antennas employed for air and coastal surveillance radars. Novel designs are introduced to obtain electronically switchable cosecant-squared and pencil beam radiation patterns, without making any changes on the reflector geometry. The analytical regularization method (ARM) is used as a fast and accurate way to solve the problem of E-polarized wave diffraction by parabolic shaped perfectly electrical conductive (PEC) cylindrical reflector with finite thickness. The numerical procedure is initially verified by the analytical and numerical methods, and the calculated radiation characteristics are presented for the proposed antenna configurations.

Index Terms - Analytical regularization method, cosecant-squared radiation pattern, multi-source horn, parabolic reflector antenna.

I. INTRODUCTION

Parabolic reflectors are one of the most popular antenna types commonly used in microwave and millimeter wave radars, power transmission, satellite communication, and navigation systems [1-4]. They have generally large physical dimensions with respect to the wavelength. Thus, high frequency electromagnetic wave scattering techniques such as, geometrical

optics (GO), physical optics (PO), aperture integration (AI), and geometric theory of diffraction (GTD) are mostly used for determining the far field antenna characteristics [5-6]. Besides, direct numerical techniques such as, method of moments (MoM), finite element method (FEM), and finite difference methods are considered more versatile and usable in practice for feeder and reflector designs [7-8]. Nevertheless, large size antenna analyses usually require long computation times [9-10]. Furthermore, MoM and FEM can cause unstable numerical processes in most cases due to reducing the boundary value problem (BVP) to the algebraic equation set of the first kind that usually has a singular kernel with a big condition number. Thus, minimizing the computational error by increasing the truncation number of the matrix-vector algebraic equation set cannot be guaranteed [11-13]. Hence, the analytical regularization method (ARM) that transforms the ill-conditioned integral equation of the first kind into a well-conditioned one of the second kind is preferred to solve the matrix equation numerically by truncation method with fast convergence to reach fast and reliable solutions [14]. The ARM solutions of the parabolic reflector structure and the H-plane horn feeder have been demonstrated separately by Turk to characterize the antenna patterns in the next step [11,16-17].

In this study, radiation characteristics of the cylindrical parabolic reflector fed by the H-plane

horn are treated parametrically to obtain pencil beam, cosecant-squared, and inverse cosecant-squared radiation patterns for air and coastal surveillance radars. For this purpose, the BVP is essentially formulated with respect to the z -component of the electric field satisfying Helmholtz's equation with Dirichlet boundary condition, and the ARM procedure is applied to obtain fast, accurate, and reliable results (see [15-17] for verification). New design proposals on mechanical switching of different beam types (pencil, cosec2, inverse cosec2) are investigated only by rotating one flare arm of the feeder horn to provide asymmetric illumination.

The final goal of the paper is achieving both pencil beam and cosecant-squared radiation patterns for one fixed reflector antenna geometry simply by electronic pin-switching of the dual-source H-plane horn feeder. By this way, both cosecant-squared and pencil beam radiation patterns can be switched electronically for the same feeder horn and reflector structure.

II. ARM FORMULATION

The parabolic reflector antenna is primarily considered as a perfectly conducting, smooth, longitudinally homogeneous and infinitely long in z -direction cylindrical obstacle, which is illuminated by the horn feeder. The XOY cross section of the structure shown in Fig. 1 is denoted by the closed contour S . If we assume the case that scalar wave does not vary along z -axis, the diffraction problem of such a scatterer object corresponds to the 2D Dirichlet boundary condition for incidence of the E-polarized wave. Thus, the incident and scattered scalar wave functions ($u^i(p)$ and $u^s(p)$) should satisfy the Helmholtz equation and the Dirichlet boundary condition given in Eq. (1) and Eq. (2), also with the Sommerfeld radiation condition (see [14]).

$$(\Delta + k^2)u^s(p) = 0, \quad p \in R^2 \setminus S, \quad (1)$$

$$u^{s(+)}(p) = u^{s(-)}(p) = -u^i(p), \quad p \in S, \quad (2)$$

where, S is the smooth contour of the structure domain in 2D space R^2 that belongs to the smoothness class $C^{2,\alpha}$ [14]. $u^{s(+)}(p)$ and $u^{s(-)}(p)$ are limiting values of $u^s(p)$ in the inner and the outer sides of the S , respectively. The Eq. (3) is the

BVP solution obtained by the Green's formula and the boundary condition in Eq. (2).

$$-\frac{i}{4} \int_S [H_0^{(1)}(k|q-p|)Z(p)] dl_p = -u^i(q), \quad q, p \in S, \quad (3)$$

$$\text{where, } Z(p) = \frac{\partial u^{s(-)}(p)}{\partial n} - \frac{\partial u^{s(+)}(p)}{\partial n} \text{ for } p \in S, \text{ and}$$

n is the unit outward with respect to S normal of the point p . The unknown function $Z(p)$ is constructed by solving Eq. (3), and using parameterization of the S contour specified by the function $\eta(\theta) = (x(\theta), y(\theta))$ that smoothly parameterizes the contour S by the points of $\theta \in [-\pi, \pi]$. Using the $\eta(\theta)$ parameterization, the integral equation representation of the first kind in Eq. (3) can be equivalently rearranged as follows:

$$\frac{1}{2\pi} \int_{-\pi}^{\pi} \left\{ \ln \left| 2 \sin \frac{\theta - \tau}{2} \right| + K(\theta, \tau) \right\} Z_D(\tau) d\tau = g(\theta), \quad (4)$$

by means of the following $\eta(\theta)$ transformations:

$$Z_D(\theta) = ([x'(\theta)]^2 + [y'(\theta)]^2)^{1/2} Z(\eta(\theta)), \quad \theta \in [-\pi, \pi] \quad (5)$$

$$|q-p| = \{[x(\theta) - x(\tau)]^2 + [y(\theta) - y(\tau)]^2\}^{1/2}, \quad \theta \in [-\pi, \pi] \quad (6)$$

$$g(\theta) = -u^i(\eta(\theta)), \quad \theta \in [-\pi, \pi]. \quad (7)$$

In Eq. (4), the unknown function is $Z_D(\tau)$, the given function is $g(\theta)$, and $K(\theta, \tau)$ function is the rather smooth section of the Green's function in comparison with the logarithmic part that contains the main singularity of this equation (see [14,15] for details). The Fourier series expansions of the functions are defined in set of Eqs. (8)-(11).

$$K(\theta, \tau) = \sum_{s=-\infty}^{\infty} \sum_{m=-\infty}^{\infty} k_{sm} e^{i(s\theta + m\tau)}, \quad \theta \in [-\pi, \pi], \quad (8)$$

$$\ln \left| 2 \sin \frac{\theta - \tau}{2} \right| = -\frac{1}{2} \sum_{\substack{n=-\infty \\ n \neq 0}}^{\infty} |n|^{-1} e^{in(\theta - \tau)}, \quad \theta \in [-\pi, \pi], \quad (9)$$

$$Z_D(\tau) = \sum_{n=-\infty}^{\infty} z_n e^{in\tau}, \quad \tau \in [-\pi, \pi], \quad (10)$$

$$g(\theta) = \sum_{n=-\infty}^{\infty} g_n e^{in\theta}, \quad \theta \in [-\pi, \pi]. \quad (11)$$

Hence, one can obtain the infinite system of the linear algebraic equations of the second kind given in Eq. (12) that guarantees the convergence and stability of the numerical process [14].

$$\hat{z}_s + \sum_{m=-\infty}^{\infty} \hat{k}_{s,m} \hat{z}_m = \hat{g}_s, \quad s = \pm 1, \pm 2, \dots \quad (12)$$

where,

$$\left. \begin{aligned} \hat{k}_{s,m} &= -2\tau_s \tau_m \left[k_{s,-m} + \frac{1}{2} \delta_{s,0} \delta_{m,0} \right] \\ \hat{z}_n &= \tau_n^{-1} z_n, \hat{g} = -2\tau_s g_s, \tau_n = \max(1, |n|^{1/2}) \end{aligned} \right\}, \quad n = 0, \pm 1, \pm 2, \dots \quad (13)$$

Finally, the scattered field $u^s(q)$ for $q \in R^2$ is calculated by the integral equation representation of the Eq. (3) with any required accuracy by using the truncation method (see [15,17] for details).

III. PARAMETRIC DESIGN OF PARABOLIC REFLECTOR ANTENNA

The ARM procedure described at Section II is derived for the investigated parabolic antenna types. The geometrical cross-section of the reflector is a modified parabolic arc, which is modeled by ARM as a closed contour L that goes from point A to point M and back to A corresponding to $\theta \in [-\pi, \pi]$, as illustrated in Fig. 1. The relation between l and θ is formulated in Eq. (14).

$$\left. \begin{aligned} l &= (\theta + \pi)L / 2\pi \\ l \in [0, L] &\rightarrow (\theta, \tau) \in [-\pi, \pi] \end{aligned} \right\}. \quad (14)$$

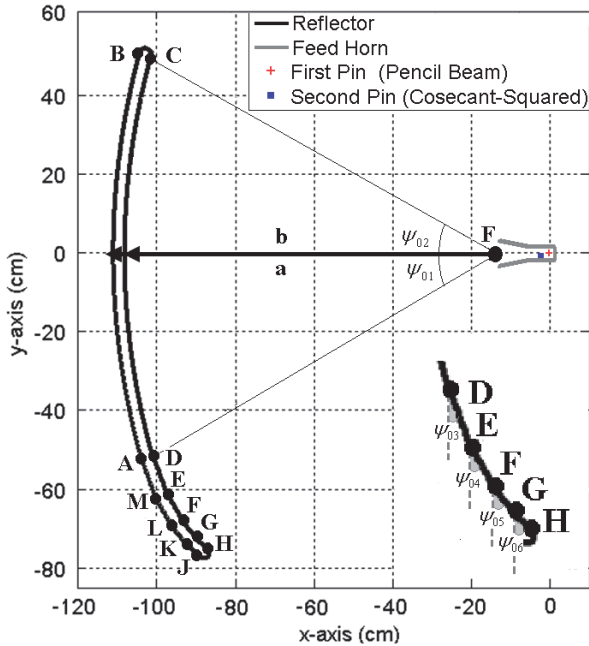


Fig. 1. XOY-plane geometry of parabolic reflector with multi-source H-plane horn feeder.

The reflector structure consists of totally 12 contour parts, which are defined in Table 1 and 2.

Table 1: Parametric definitions of reflector contour

No	Region	Definition
1	AB	$-\pi \leq \theta < -\pi + 2L_{AB} \pi/L$
2	BC	$-\pi + 2L_{AB} \pi/L \leq \theta < -\pi + 2L_{BC} \pi/L$
3	CD	$-\pi + 2L_{BC} \pi/L \leq \theta < -\pi + 2L_{CD} \pi/L$
4	DE	$-\pi + 2L_{CD} \pi/L \leq \theta < -\pi + 2L_{DE} \pi/L$
5	EF	$-\pi + 2L_{DE} \pi/L \leq \theta < -\pi + 2L_{EF} \pi/L$
6	FG	$-\pi + 2L_{EF} \pi/L \leq \theta < -\pi + 2L_{FG} \pi/L$
7	GH	$-\pi + 2L_{FG} \pi/L \leq \theta < -\pi + 2L_{GH} \pi/L$
8	HJ	$-\pi + 2L_{GH} \pi/L \leq \theta < -\pi + 2L_{HJ} \pi/L$
9	JK	$-\pi + 2L_{HJ} \pi/L \leq \theta < -\pi + 2L_{JK} \pi/L$
10	KL	$-\pi + 2L_{JK} \pi/L \leq \theta < -\pi + 2L_{KL} \pi/L$
11	LM	$-\pi + 2L_{KL} \pi/L \leq \theta < -\pi + 2L_{LM} \pi/L$
12	MA	$-\pi + 2L_{LM} \pi/L \leq \theta < \pi$

Table 2: Segment lengths of the contour regions

No	Region	Segment Length
1	AB	$L_{AB} = b \tan((\psi_{02} - \psi_{01}) / 2)$
2	BC	$L_{BC} = L_{AB} + \pi c_2$
3	CD	$L_{CD} = L_{BC} + a \tan((\psi_{02} - \psi_{01}) / 2)$
4	DE	$L_{DE} = L_{CD} + c_3$
5	EF	$L_{EF} = L_{DE} + 0.75c_3$
6	FG	$L_{FG} = L_{EF} + 0.5c_3$
7	GH	$L_{GH} = L_{FG} + 0.25c_3$
8	HJ	$L_{HJ} = L_{GH} + \pi c_1$
9	JK	$L_{JK} = L_{HJ} + 0.25c_3$
10	KL	$L_{KL} = L_{JK} + 0.5c_3$
11	LM	$L_{LM} = L_{KL} + 0.75c_3$
12	MA	$L = L_{LM} + c_3$

* $c_1 = (b - a) / (1 + \cos(\psi_{01}))$, $c_2 = (b - a) / (1 + \cos(\psi_{02}))$, $c_3 = 4\lambda$

The parameterization of the contour line is implemented separately from point A to M , and back to A by means of the variable $l \in [0, L]$ as follows:

$$x = \frac{-2b \cos \varphi_{01}}{1 + \cos \varphi_{01}} - X_s, \quad y = \frac{2b \sin \varphi_{01}}{1 + \cos \varphi_{01}}, \quad l \in [AB], \quad (15)$$

$$\left. \begin{aligned} x &= c_2 \cos\left(\frac{-l + L_{AB} + \pi - \psi_{02}}{c_2}\right) - \frac{(a+b) \cos \psi_{02}}{1 + \cos \psi_{02}} - X_s \\ y &= c_2 \sin\left(\frac{-l + L_{AB} + \pi - \psi_{02}}{c_2}\right) + \frac{(a+b) \sin \psi_{02}}{1 + \cos \psi_{02}} \end{aligned} \right\}, \quad l \in [BC], \quad (16)$$

$$x = \frac{-2a \cos \varphi_{02}}{1 + \cos \varphi_{02}} - X_s, \quad y = \frac{2a \sin \varphi_{02}}{1 + \cos \varphi_{02}}, \quad l \in [CD], \quad (17)$$

$$\left. \begin{aligned} x &= \frac{-2a \cos \psi_{01}}{1 + \cos \psi_{01}} + (l - L_{CD}) \cos \psi_{03} - X_s \\ y &= \frac{2a \sin \psi_{01}}{1 + \cos \psi_{01}} - (l - L_{CD}) \sin \psi_{03} \end{aligned} \right\}, \quad l \in [DE], \quad (18)$$

$$\left. \begin{aligned} x &= \frac{-2a \cos \psi_{01}}{1 + \cos \psi_{01}} + c_3 \cos \psi_{03} + (l - L_{DE}) \cos \psi_{04} - X_s \\ y &= \frac{2a \sin \psi_{01}}{1 + \cos \psi_{01}} - c_3 \sin \psi_{03} - (l - L_{DE}) \sin \psi_{04} \end{aligned} \right\}, \quad l \in [EF], \quad (19)$$

$$\left. \begin{aligned} x &= \frac{-2a \cos \psi_{01}}{1 + \cos \psi_{01}} + (l - L_{EF}) \cos \psi_{05} - X_s \\ &\quad + c_3 (\cos \psi_{03} + 0.75 \cos \psi_{04}) \\ y &= \frac{2a \sin \psi_{01}}{1 + \cos \psi_{01}} - (l - L_{EF}) \sin \psi_{05} \\ &\quad - c_3 (\sin \psi_{03} + 0.75 \sin \psi_{04}) \end{aligned} \right\}, \quad l \in [FG], \quad (20)$$

$$\left. \begin{aligned} x &= \frac{-2a \cos \psi_{01}}{1 + \cos \psi_{01}} + (l - L_{FG}) \cos \psi_{06} - X_s \\ &\quad + c_3 (\cos \psi_{03} + 0.75 \cos \psi_{04} + 0.5 \cos \psi_{05}) \\ y &= \frac{2a \sin \psi_{01}}{1 + \cos \psi_{01}} - (l - L_{FG}) \sin \psi_{06} \\ &\quad - c_3 (\sin \psi_{03} + 0.75 \sin \psi_{04} + 0.5 \sin \psi_{05}) \end{aligned} \right\}, \quad l \in [GH], \quad (21)$$

$$\left. \begin{aligned} x &= c_1 \cos \left(\frac{-l + L_{GH}}{c_1} - \psi_{01} \right) - \frac{(a+b) \cos \psi_{01}}{1 + \cos \psi_{01}} - X_s \\ &\quad + c_3 (\cos \psi_{03} + 0.75 \cos \psi_{04} + 0.5 \cos \psi_{05} + 0.25 \cos \psi_{06}) \\ y &= c_1 \sin \left(\frac{-l + L_{GH}}{c_1} - \psi_{01} \right) + \frac{(a+b) \sin \psi_{01}}{1 + \cos \psi_{01}} \\ &\quad - c_3 (\sin \psi_{03} + 0.75 \sin \psi_{04} + 0.5 \sin \psi_{05} + 0.25 \sin \psi_{06}) \end{aligned} \right\}, \quad l \in [HI], \quad (22)$$

$$\left. \begin{aligned} x &= c_1 \cos(\pi + \psi_{01}) - \frac{(a+b) \cos \psi_{01}}{1 + \cos \psi_{01}} - (l - L_{IJ}) \cos \psi_{06} - X_s \\ &\quad + c_3 (\cos \psi_{03} + 0.75 \cos \psi_{04} + 0.5 \cos \psi_{05} + 0.25 \cos \psi_{06}) \\ y &= c_1 \sin(-\pi - \psi_{01}) + \frac{(a+b) \sin \psi_{01}}{1 + \cos \psi_{01}} + (l - L_{IJ}) \sin \psi_{06} \\ &\quad - c_3 (\sin \psi_{03} + 0.75 \sin \psi_{04} + 0.5 \sin \psi_{05} + 0.25 \sin \psi_{06}) \end{aligned} \right\}, \quad l \in [JK], \quad (23)$$

$$\left. \begin{aligned} x &= c_1 \cos(\pi + \psi_{01}) - \frac{(a+b) \cos \psi_{01}}{1 + \cos \psi_{01}} - (l - L_{JK}) \cos \psi_{05} - X_s \\ &\quad + c_3 (\cos \psi_{03} + 0.75 \cos \psi_{04} + 0.5 \cos \psi_{05}) \\ y &= c_1 \sin(-\pi - \psi_{01}) + \frac{(a+b) \sin \psi_{01}}{1 + \cos \psi_{01}} + (l - L_{JK}) \sin \psi_{05} \\ &\quad - c_3 (\sin \psi_{03} + 0.75 \sin \psi_{04} + 0.5 \sin \psi_{05}) \end{aligned} \right\}, \quad l \in [KL], \quad (24)$$

$$\left. \begin{aligned} x &= c_1 \cos(\pi + \psi_{01}) - \frac{(a+b) \cos \psi_{01}}{1 + \cos \psi_{01}} - X_s \\ &\quad + c_3 (\cos \psi_{03} + 0.75 \cos \psi_{04}) - (l - L_{KL}) \cos \psi_{04} \\ y &= c_1 \sin(-\pi - \psi_{01}) + \frac{(a+b) \sin \psi_{01}}{1 + \cos \psi_{01}} \\ &\quad - c_3 (\sin \psi_{03} + 0.75 \sin \psi_{04}) + (l - L_{KL}) \sin \psi_{04} \end{aligned} \right\}, \quad l \in [LM], \quad (25)$$

$$\left. \begin{aligned} x &= c_1 \cos(\pi + \psi_{01}) - \frac{(a+b) \cos \psi_{01}}{1 + \cos \psi_{01}} - X_s \\ &\quad + c_3 \cos \psi_{03} - (l - L_{LM}) \cos \psi_{03} \\ y &= c_1 \sin(-\pi - \psi_{01}) + \frac{(a+b) \sin \psi_{01}}{1 + \cos \psi_{01}} \\ &\quad - c_3 \sin \psi_{03} + (l - L_{LM}) \sin \psi_{03} \end{aligned} \right\}, \quad l \in [MA], \quad (26)$$

where, $X_s = 5.243\lambda$ and,

$$\varphi_{01} = \psi_{01} + [(\psi_{02} - \psi_{01})l / L_{AB}], \quad (27)$$

$$\varphi_{02} = \psi_{02} - [(\psi_{02} - \psi_{01})(l - L_{BC}) / (L_{CD} - L_{BC})]. \quad (28)$$

The horn feeder model illustrated in Fig. 1 is assumed to be located at the focus of the PEC reflector antenna. On this scope, the near field distribution of the feed horn, which corresponds to the incident wave, is calculated firstly by using the ARM to determine the illumination pattern on the reflector surface [16].

IV. ANTENNA DESIGNS AND NUMERICAL RESULTS

A. Verification of ARM performance

The parametric analyses of the various types of reflector antennas are focused on obtaining both pencil-beam and cosecant-squared radiation patterns. The main idea of this paper is to improve the air scanning performance of air surveillance microwave radars to detect aircrafts approaching with the right angles towards to radar system. Before demonstrating the numerical results, it is important to explain the reliability of the generic ARM algorithm, which has already been verified with analytical results by achieving very good coherency for the cases of plane wave scattering from a circular cylinder, radiation from open ended waveguide, and two horn types [see 11, 16, 17, respectively]. The ARM solution of 10λ diameter (30cm at 10GHz) parabolic reflector antenna was also compared with 3D MoM simulator, and the good agreement was observed in Fig. 2.

The convergence behavior of the numerical process is highly important for the algorithm performance, as it is strictly related to the stability and processing time of the solution. The average relative computation error on the gain pattern plotted in Fig. 3 implies that ARM is a useful and reliable numerical technique due to fast

convergence and short calculation times (see also Table 3), especially for large size design and wide band analysis of the parabolic antennas.

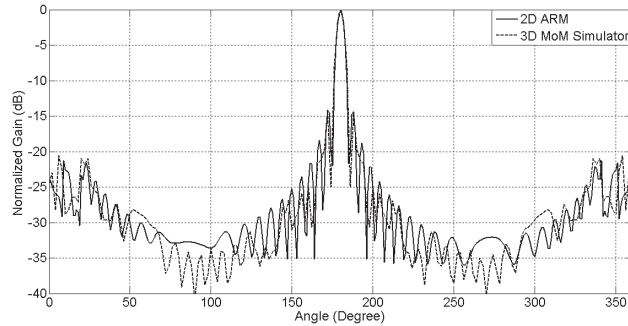


Fig. 2. Comparison of radiation patterns calculated by 2D ARM and 3D MoM simulator.

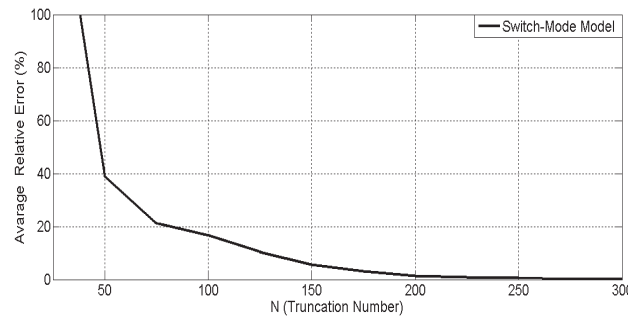


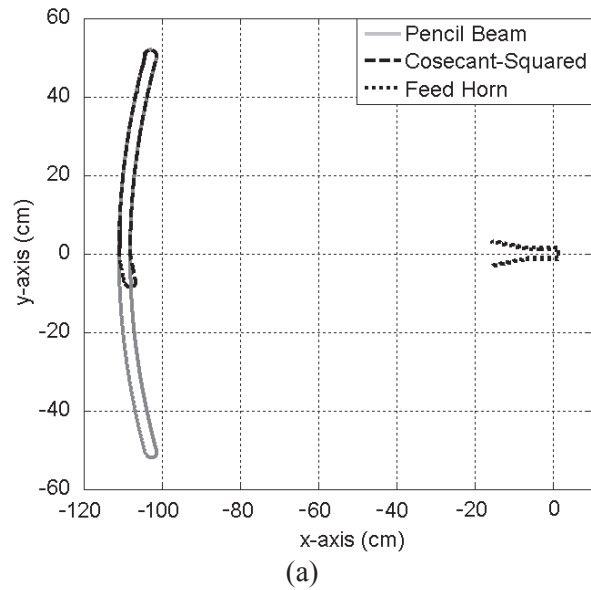
Fig. 3. Average of relative errors in numerical calculations vs. number of segments.

Table 3: Computation times of ARM and 3D MoM simulator (2.8 GHz, 4 GB RAM)

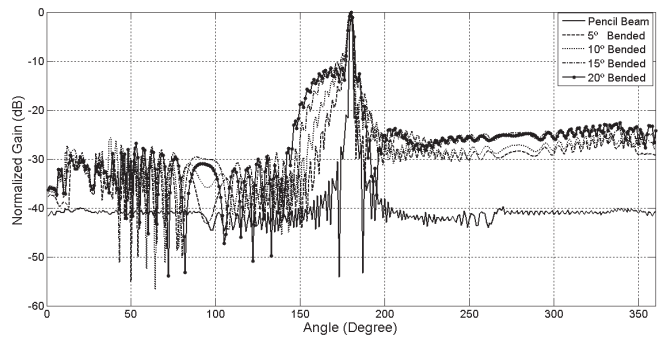
Truncation Number (N)	Computation Time	
	2D ARM	3D MoM
25	5 sec.	20 h.
50	34 sec.	
75	1.5 min.	
100	4 min.	
150	14 min.	
200	25 min.	
300	1.5 h.	
600	11 h.	

B. Analysis of cut-bended reflector model

At the first conventional design structure, the bottom side of classic reflector geometry is cut partially and bended by 5°, 10°, 15°, and 20°, respectively, in order to obtain cosecant-squared radiation pattern. The effects of these parameters on the far field antenna characteristics are analyzed by ARM, and the radiation patterns are demonstrated in Fig. 4. It can be clearly seen that a more bending angle is needed to reach more expanded beam on the radiation pattern. Nevertheless, it is also observed that if we bend the bottom part of the reflector over 20° the radiation pattern tends to bifurcate.



(a)



(b)

Fig. 4. (a) XOY-plane cross section of cut-bended reflector; (b) normalized radiation patterns of the structure for different bending angles (f= 10GHz).

C. Analysis of convex reflector model

In the second structure, the upper side of the reflector antenna is designed as convex to obtain cosecant-squared radiation pattern, and it is bended outwards by 5° , 10° , and 15° , respectively. It is seen at Fig. 5 that the expanding angle of the radiation pattern increases as the bending angle is increasing. However similarly, it starts to bifurcate if the convex part is bended over 15° .

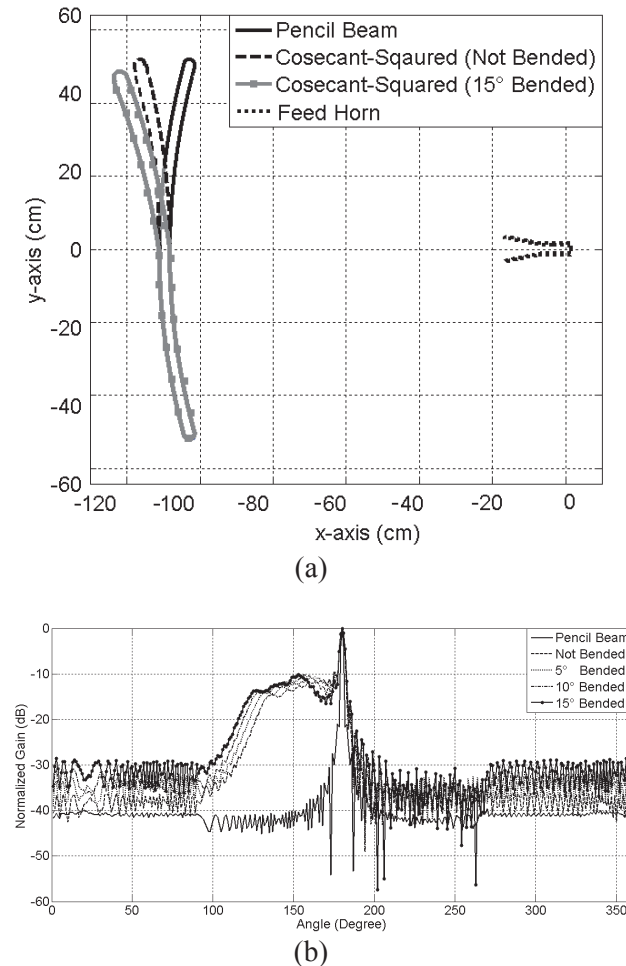


Fig. 5. (a) XOY-plane cross section of convex reflector; (b) normalized radiation patterns of the structure for different bending angles ($f=10\text{GHz}$).

D. Design proposal by using asymmetric feed horn

For the aim of obtaining both pencil beam and cosecant-squared radiation patterns for the same reflector geometry, an additional cascade part with different lengths is added to the bottom of the classic reflector structure (see Fig. 1), and the antenna is illuminated by using symmetric (solid) and asymmetric (dashed) flare H-plane horn

feeders as illustrated in Fig. 6a. Typical pencil beam and cosecant-squared radiation patterns can be switched just by arranging the lower flare angle of the feed horn as 11.18° (solid) and 70° (dashed), respectively. In this way, the amplitude of illumination on the cascade part, which reflects the incident signal upwards instead of into parallel, increases so that a cosecant-squared radiation pattern can appear, as shown in Fig. 6b.

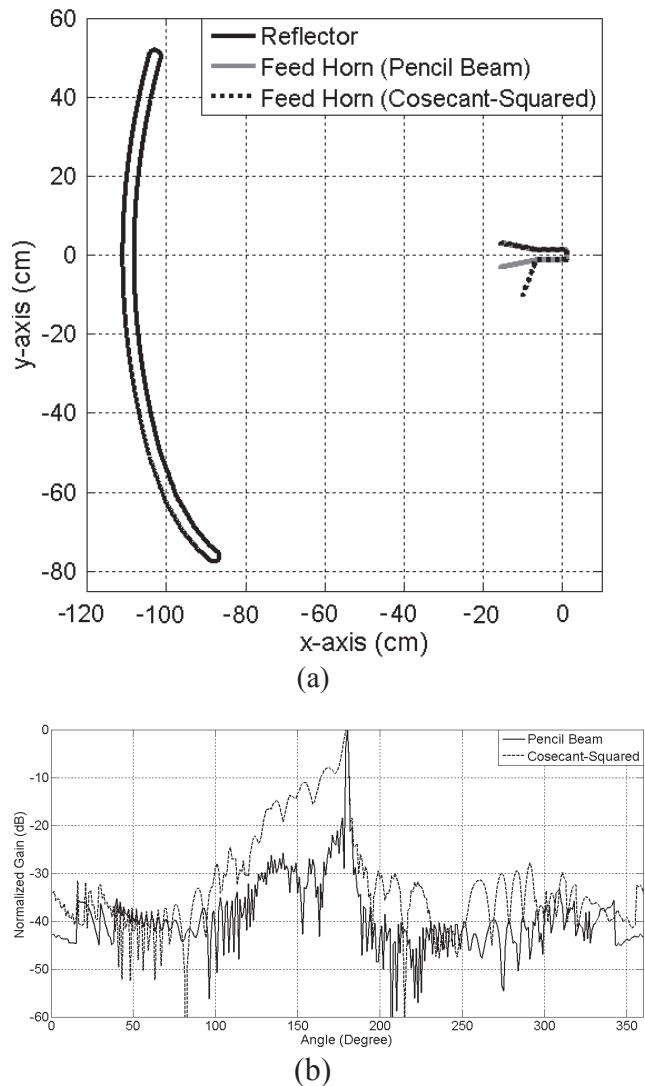


Fig. 6. (a) XOY-plane cross section of the reflector fed by symmetric and asymmetric feed horn; (b) normalized radiation patterns at $f=10\text{GHz}$.

E. Design proposal by using switch-mode feed horn

This is the final design proposal with double-source feed horn located at the focus of the PEC reflector (see Fig. 1). The analysis procedure is

concentrated on obtaining both pencil beam and cosecant-squared radiation patterns without changing the geometry of feed horn and reflector antennas. In this context, if the first monopole pin of the horn located at the origin is switched on, the feed horn illuminates the reflector aperture to yield a typical pencil beam radiation pattern. In the case of switching on the second monopole pin of the horn located at coordinates $x= 1.1\lambda$, $y= -0.3\lambda$, a typical cosecant-squared radiation pattern is observed. Figure 7 exhibits the effects of pin switching between two sources of the H-plane feed horn antenna to achieve both pencil beam and cosecant-squared radiation patterns with the same feed horn and reflector geometries.

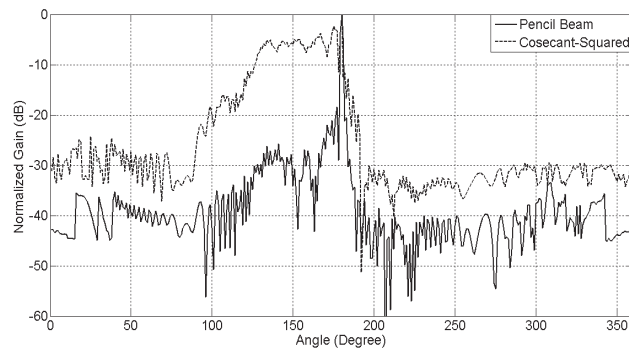


Fig. 7. Normalized radiation patterns of the switch-mode reflector antenna design at $f= 10\text{GHz}$ (Solid line: pin 1 is ON, Dashed line: pin 2 is ON).

V. CONCLUSION

In this paper, radiation characteristics of the cylindrical parabolic reflector fed by H-plane horn are investigated parametrically to obtain pencil beam and cosecant-squared radiation patterns for air and coastal surveillance radars. Novel antenna designs are proposed to achieve switchable pencil beam and cosecant-squared radiation patterns without making any changes on the antenna geometries. Furthermore, some common cosecant-squared reflector geometries such as, cut-bended and convex shapes, are also analyzed by using the analytical regularization method, which is fast and reliable numerical-analytical technique. After verification, the analysis results of the designed reflector structures are demonstrated on the radiation patterns.

The main goal of this work in practice is to improve the air scanning performance of air and coastal surveillance radars to enable them to detect aircrafts drifting towards to radar at right angles.

REFERENCES

- [1] M. I. Skolnik, "Radars Handbook," 2nd ed., McGraw-Hill, 1990.
- [2] J. L. Volakis, *Antenna Engineering Handbook*, 4th ed., McGraw-Hill, 2007.
- [3] S. Rao, M. Tang, and C. Hsu, "Multiple Beam Antenna Technology for Satellite Communications Payloads," *Applied Computational Electromagnetic Society (ACES) Journal*, vol. 21, no. 3, pp. 353-364, November 2006.
- [4] T. Uno and S. Adachi, "Optimization of Aperture Illumination for Radio Wave Power Transmission," *IEEE Trans. Antennas and Propagation*, vol. 32, pp. 628-632, 1984.
- [5] K. Tap and P. H. Pathak, "A Fast Hybrid Asymptotic and Numerical Physical Optics Analysis of Very Large Scanning Cylindrical Reflectors with Stacked Linear Array Feeds," *IEEE Trans. Antennas and Propagation*, vol. 54, no. 4, pp. 1142-1151, 2006.
- [6] M. Djordjevic and B. M. Notaros, "Higher Order Hybrid Method of Moments-Physical Optics Modeling Technique for Radiation and Scattering from Large Perfectly Conducting Surfaces," *IEEE Trans. Antennas and Propagation*, vol. 53, no. 2, pp. 800-813, 2005.
- [7] K. Umashankar and A. Taflove, "Computational Electromagnetics," Artech House, 1993.
- [8] V. P. Chumachenko, A. S. Turk, "Radiation Characteristics of Wide-Angle H-Plane Sectoral Horn Loaded with Dielectric of Multi-Angular Shape," *Int. Journal Electronics*, vol. 88, no. 1, pp. 91-101, 2001.
- [9] F. Arndt, J. Brandt, V. Catina, J. Ritter, I. Rullhusen, J. Dauelsberg, U. Hilgefert, and W. Wessel, "Fast CAD and Optimization of Waveguide Components and Aperture Antennas by Hybrid MM/FE/MoM/FD Methods: State of the Art and Recent Advances," *IEEE Trans. Microwave Theory Tech.*, vol. 52, no.1, 2004.
- [10] W. Ewe, L. Li, Q. Wu, and M. Leong, "Analysis of Reflector and Horn Antennas using Adaptive Integral Methods," *IEICE Trans. Comm.*, vol. E88-B, no. 6, 2005.
- [11] A. S. Turk, "Analysis of Aperture Illumination and Edge Rolling Effects for Parabolic Reflector Antenna Design,"

International Journal of Electronics and Comm. (AEUE), vol. 60, pp. 257-266, 2006.

- [12] J. H. Wilkinson, “*The Algebraic Eigenvalue Problem*,” Clarendon Press, Oxford, 1965.
- [13] C. A. J. Fletcher, “*Computational Galerkin Method*,” Springer-Verlag, Berlin, 1984.
- [14] Yu. A. Tuchkin, “Wave Scattering by an Open Cylindrical Screen of Arbitrary Profile with Dirichlet Boundary Value Condition,” *Soviet Physics Doklady*, vol. 30, pp. 1027-1030, 1985.
- [15] E. Karacuha, A. S. Turk, “E-Polarized Scalar Wave Diffraction by Perfectly Conductive Arbitrary Shaped Cylindrical Obstacles with Finite Thickness,” *Int. J. Infrared and Millimeter Waves*, vol. 22, pp. 1531-1546, 2001.
- [16] A. S. Turk, O. M. Yucedag, and O. Yurduseven, “Parametric Analysis of H-Plane Horn Antenna Radiation,” *Proc. 7th International Kharkov Symposium on Physics and Engineering of Microwaves, Millimeter and Sub-millimeter Waves (MSMW)*, IEEE press, Kharkov, Ukraine, pp. 21-26 June 2010.
- [17] A. S. Turk and O. Yurduseven, “Parametric Analysis of Multi-Source Feeding Flare Rolling and Corrugating Effects for H-Plane Horn Radiator,” *Applied Computational Electromagnetic Society (ACES) Journal*, vol. 25, no.1, January, 2011.



Ahmet Serdar Turk received the B.Sc. degree in Electronics-Communication Engineering from Yıldız Technical University, Istanbul, Turkey in 1996. He received the M.Sc. and Ph.D. degrees in Electronics Engineering from Gebze Institute of Technology, Kocaeli, Turkey in 1998 and 2001, respectively. He joined the Scientific and Technical Research Council of Turkey (TUBITAK) in 1998.

He has been working on land mine detection systems as an impulse radar RF system and antenna designer since 1998. His research interests include horn, reflector, array, and ultra-wide band antenna designs in RF and microwave bands, numerical methods in electromagnetic wave scattering, high frequency surface wave radar,

ground penetrating radar, and microwave and millimeter wave radar systems.

He is currently working as associated professor at Yıldız Technical University.



Okan Yurduseven received the B.Sc. degree in Electronics-Communication Engineering from Yıldız Technical University, Istanbul, Turkey in 2009. He is currently working as research assistant in the Department of Electrical and Electronics Engineering at Marmara University, Istanbul, Turkey. His current research interests are in the areas of electromagnetic fields and waves, microwaves, antennas and propagation, radar systems, radar cross section, and numerical methods in electromagnetic theory.